

Colloid Retention in Porous Media: Mechanistic Confirmation of Wedging and Retention in Zones of Flow Stagnation

W. P. JOHNSON,* XIQING LI, AND GOZDE YAL

Department of Geology and Geophysics, University of Utah, Salt Lake City, Utah 84112

A three-dimensional particle tracking model for colloid transport in porous media was developed that predicts colloid retention in porous media in the presence of an energy barrier via two mechanisms: (1) wedging of colloids within grain to grain contacts; (2) retention of colloids (without attachment) in flow stagnation zones. The model integrates forces experienced by colloids during transport in porous media, i.e., fluid drag, gravity, diffusion, and colloid–surface Derjaguin–Landau–Verwey–Overbeek interactions. The model was implemented for a fluid flow field that explicitly represented grain to grain contacts. The model utilized a variable time stepping routine to allow finer time steps in zones of rapid change in fluid velocity and colloid–surface interaction forces. Wedging was favored by colloid: collector ratios greater than about 0.005, with this threshold ratio increasing with decreasing fluid velocity. Retention in flow stagnation zones was demonstrated for colloid: collector ratios less than about 0.005, with this threshold decreasing with increasing fluid velocity. Both wedging and retention in flow stagnation zones were sensitive to colloid–surface interaction forces (energy barrier height and secondary energy minimum depth). The model provides a mechanistic basis for colloid retention in the presence of an energy barrier via processes that were recently hypothesized to explain experimental observations.

Introduction

That colloid deposition occurs in porous media despite the expected presence of formidable energy barriers to deposition is an important benefit to water resource protection and water treatment strategies. The inability of classic filtration theory to reflect this experience is also an important challenge to researchers concerned with the transport of colloids in porous media. Potential mechanisms of colloid deposition in the presence of an energy barrier to attachment have been elucidated in a number of publications during the past several decades. Among them are the following: (1) surface charge heterogeneity and roughness at which the energy barrier to deposition is locally reduced or eliminated (1–4); (2) straining of colloids in pore constrictions too small to pass (5–11); and more recently, (3) the presence of flow stagnation zones within which colloids are retained without direct contact with the surface, but in association with the surface via secondary energy minima (12–18).

The first mechanism (surface heterogeneity) has received the greatest attention possibly because it is the most obvious mechanism in the context of classic filtration theory. In classic filtration theory, the porous media is idealized as a bed of spherical collectors (grains) each completely surrounded by a sheath of fluid (Happel sphere). Colloids transported within the sheath of fluid surrounding the idealized collector may intercept the surface either by virtue of the fluid stream line they follow or by crossing fluid stream lines due to diffusion and settling. In this classic model, retention upon close approach of the colloid to the collector surface occurs if it is allowed by the net colloid–collector interaction energy, which is classically composed of van der Waals and electric double layer interactions. When both interactions are attractive, there is no barrier to attachment, and colloids that closely approach collector surfaces are attached (assuming steric repulsion is absent). In many environmental contexts, however, the electric double layer interaction is repulsive, yielding an energy barrier to attachment of magnitude that depends on the colloid and collector surface charges as well as solution characteristics such as pH and ionic strength. According to simulations using the classic Happel sphere, colloid attachment is prevented in the presence of an energy barrier greater than a few kT (e.g., 1), whereas colloid deposition occurs on surfaces with like (same sign of) charge as the colloid despite painstaking efforts to remove impurities (e.g., 14, 19). A valuable body of research has been generated demonstrating that surface charge heterogeneity and nanoscale roughness can reduce or eliminate the energy barrier that would otherwise be expected (e.g., 1–4).

That surface heterogeneity alone cannot account for colloid retention in porous media in the presence of an energy barrier is demonstrated by comparison of deposition efficiencies in porous media relative to flat surfaces under equivalent experimental conditions, where an impinging jet reflects the forward stagnation zone of a spherical collector (flow is directed normal to the surface). Comparisons demonstrate that, under equivalent conditions, deposition efficiencies are greater in porous media relative to impinging jets, e.g., by factors of 2–50 or more for a wide range of colloid sizes (100 nm to 2 μ m), with the ratio depending on colloid size, grain size, grain angularity, and fluid velocity (15). Much of this “excess” deposition is reversible with respect to ionic strength, that is, a majority of the retained colloids are released upon introduction of low ionic strength solution, thereby implicating the secondary energy minimum as the mechanism of association of the colloids with the grain surfaces (16–18). Since colloids associated with surfaces via the secondary energy minimum are subject to hydrodynamic drag, the ultimate locations of retention of secondary-minimum associated colloids are expected to be flow stagnation zones in the porous media (12–15, 20).

The potential importance of straining as a colloid deposition mechanism is well described (8–11, 21). More recently, wedging of colloids in grain to grain contacts was identified as a potentially important mechanism of colloid deposition via direct observation (22, 23). Notably, attached colloids were distributed evenly across the collector surfaces in the absence of an energy barrier, whereas deposition occurred dominantly at grain to grain contacts in the presence of an energy barrier.

The above observations regarding excess deposition efficiency via wedging and flow stagnation beg theoretical investigation of the potential role of these processes in porous media. Cushing and Lawler (24) developed a three-dimensional particle tracking model (with explicit rendering of grain

* Corresponding author phone: (802) 581-5033; fax: (801) 581-7065; e-mail: wjohnson@earth.utah.edu.

to grain contacts) yielding significant colloid deposition in the presence of an energy barrier. However, the model also displayed insensitivity to energy barrier height, weakening confidence that the model accurately represented deposition process in porous media in the presence of an energy barrier. Unit collectors that have been examined other than the Happel sphere include the two-dimensional constricted tube model (25, 26). A three-dimensional version of the constricted tube model was more recently developed (27–29); however, the unit collector geometry involved a smooth parabolic constriction (e.g., venturi) rather than a geometry leading toward a singularity, as occurs at grain to grain contacts. Following on the pioneering work of Cushing and Lawler (24), the objective of this paper is to demonstrate the mechanistic basis for colloid retention in porous media in the presence of an energy barrier using a particle trajectory model that accounts for the various forces acting on the colloid in a flow field accounting for grain to grain contacts, i.e., fluid drag, gravity, colloidal interaction, and diffusion.

Methods

Pore Domain. Two porous media packing structures, simple cubic (SC) packing and dense cubic (DC) packing were examined in the simulations (Supporting Information). The simple and dense cubic packing structures yield porosities (0.476 and 0.260, respectively) that bracket the porosity of the porous media used in our corresponding experiments (0.375).

For both packing structures, unit cells were chosen for two different entry (and exit) planes, which were $z = 0$ or $z = 1$ (SC), and $z = -1.414$ or $z = 0$ (DC), where the coordinate values were normalized to the collector (grain) radius. The x – y boundaries on the unit collectors were -1 to 1 for the DC unit collector, and were 0 to 2 for the SC unit collector (Supporting Information).

Fluid Flow Field. The x – y – z components of the fluid velocities (v_x , v_y , v_z) are known throughout the unit collector domains via closed form solutions (trial functions) developed for the DC unit collector (30) and the SC unit collector (31). The trial functions yield dimensionless components of the fluid velocities (v_x^* , v_y^* , v_z^*), which are converted to their dimensional counterparts using the following relationships:

$$v_i = v_i^*(100.3v_s) \quad \text{for the SC unit collector}$$

$$v_i = v_i^*(3875.97v_s) \quad \text{for the DC unit collector}$$

where the subscript i refers to the x -, y -, or z -dimension, v_s is the superficial fluid velocity (Darcy velocity) in the unit collector, and the coefficients 100.3 and 3875.97 represent the relationship between pressure drop, collector radius, fluid viscosity, and superficial velocity within the unit collector as given in Sorenson and Stewart (31) and Snyder and Stewart (30), respectively. Additional discussion of the flow fields is provided in the Supporting Information.

Forces. The x – y – z components of the colloid velocity (u_x , u_y , u_z) are determined by integration of forces that may influence colloid motion in each of the three dimensions, including the following: virtual mass, gravity, electric double layer, van der Waals, Brownian, driving fluid drag, and resisting fluid drag, as described in detail in the Supporting Information.

The driving fluid drag force is influenced by hydrodynamic retardation at close proximity to the impinging surface (32–35). Hydrodynamic retardation of the colloid results from expulsion of fluid between the approaching surfaces, and is represented by a set of hydrodynamic functions that are cast in dimensions normal (n) or tangential (t) to the collector surface, requiring resolution of normal and tangential forces

into their x -, y -, and z -components, as described in detail in the Supporting Information.

Boundaries. A user-specified number of particles (e.g., 1000) were released randomly over the entry plane of the unit collectors. Initial x – y positions in the entry plane were disallowed if the particle would penetrate the collector surface. When colloids passed through one of the bounding x - or y -planes in the unit collector, the colloid was placed within the unit collector at an equivalent position to that which the colloid would have had in the adjacent unit collector. When colloids approached within 1 nm of the collector surface, the calculated van der Waals attraction dominated under all conditions, and the particle was considered attached. The colloid was considered to remain within the system when the particle residence time exceeded the user-input experimental time. To minimize computational time, an algorithm was added to recognize nonattached colloids retained in flow stagnation zones. To determine lack of significant net motion, the algorithm determined the average translation per time step for the first 5 s. If subsequent translations per time step were lower than this value, the corresponding location was noted. If the corresponding location did not change more than 10 micrometers within 200 s, the particle was considered retained despite not being attached to the surface. Simulations were run using a total simulation time twice greater than the injection duration in order to ensure that all translating particles could exit before the end of the simulation. The above initial and boundary conditions are described in greater detail in the Supporting Information.

Simulated Conditions. To reflect experimental conditions used by Tong and Johnson (15) and Li et al., (36), the simulations were performed using a collector grain radius of 255 μm and colloid radii in the range from 0.1 and 10.0 μm . Selected additional simulations used a collector radius of 390 μm and colloid radius of 18 μm to reflect the experimental conditions of Li et al. (23). Superficial fluid velocities ranged between 8.5×10^{-6} and 4.0×10^{-4} m s^{-1} in all simulations. The densities of the colloids were 1055 and 1160 g cm^{-3} for microspheres with radii < 18 μm and 18 μm , respectively. The values for the ζ -potentials used in the simulations were -60 mV for the collector surfaces and $+20$ or -20 mV for the colloid surface in the absence versus the presence of an energy barrier, respectively. The ionic strength used for simulations in the absence of an energy barrier was 0.02 M, whereas the ionic strengths used for simulations in the presence of an energy barrier were 0.001 and 0.02 M. The combined glass–water–microsphere Hamaker constants were 3.84×10^{-21} and 2.62×10^{-20} J for microspheres with radii < 18 μm and 18 μm , respectively, with the difference reflecting the different compositions of the < 18 μm (carboxylate modified polystyrene latex) and 18 μm (gold-coated hollow glass microspheres) (Supporting Information). The simulations were run using an injection time of 1200 s, followed by an elution time of 2400 s.

Time Step Management and Parallelization. The simplicity of the particle tracking approach allowed an adaptive time stepping strategy that ensured the force and velocity did not change beyond a prescribed tolerance during each time step, as described in detail in the Supporting Information. A single particle trajectory required simulation times ranging between seconds to days depending on experimental conditions being simulated, and the colloid–surface separation distances experienced on the trajectory. For nearly all simulations, 1000 particle trajectories were examined. For several of the simulations, less than one thousand trajectories were simulated due to the extremely large run times required to resolve the trajectories under the conditions examined. For example, 0.02 M ionic strength conditions in the presence of an energy barrier yielded large run times since significant

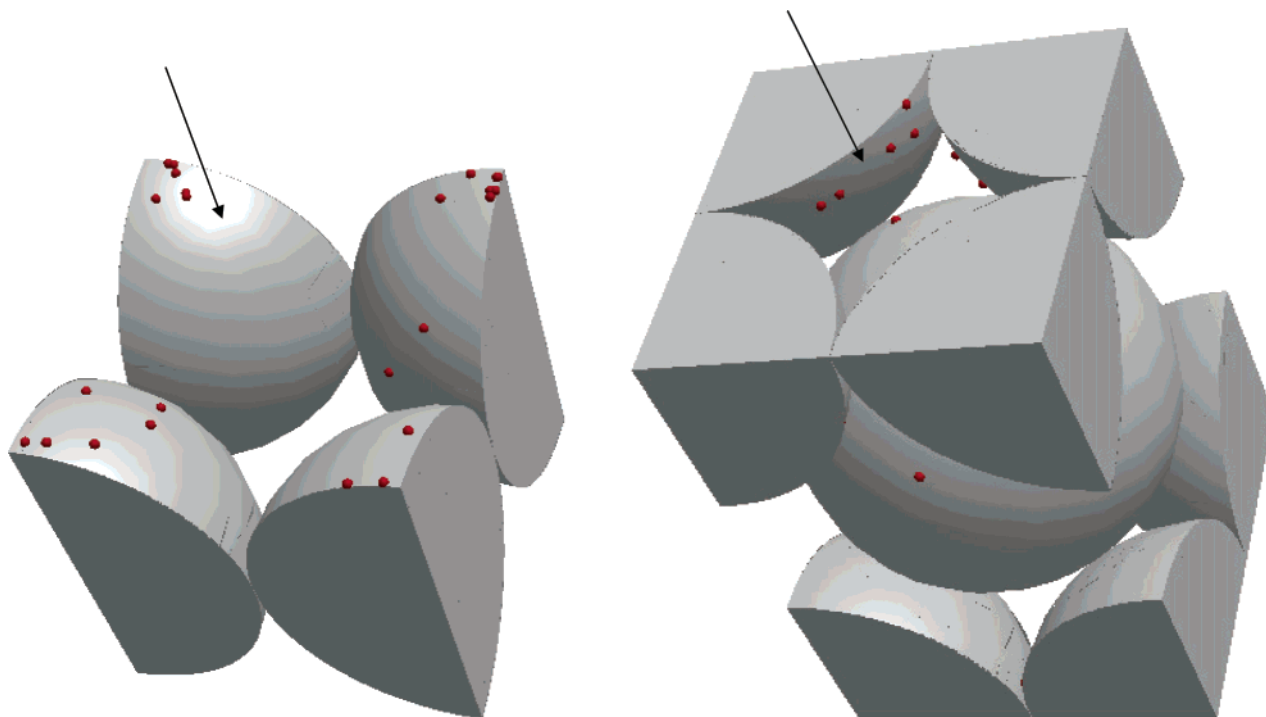


FIGURE 1. Distribution of attached colloids in the absence of an energy barrier to deposition in the SC unit collector (entry plane $z = 1$) (left) and the DC unit collector (entry plane $z = -1.414$) (right). The distribution was developed by superimposing locations of attachment determined in the simulations onto the unit collectors. Arrows denote directions of flow in z -dimension. Colloid and collectors are not proportionally scaled.

numbers of colloids translated near collector surfaces in the secondary energy minimum. The simulations were run for sufficiently long run times to ensure that unresolved particles did not contain information that would significantly affect the simulated results. Due to the long run times, simulations were run on 20 processors simultaneously with support from the Center for High Performance Computing at the University of Utah.

Results

Absence of Energy Barrier. Simulated collector efficiencies (η) are provided in tabular form in the Supporting Information. The influence of porous media packing structure on the collector efficiency (η) was significant, with more than an order of magnitude difference in the simulated values of η using the SC and DC unit collectors under equivalent conditions (Supporting Information), highlighting the dependence of η on the unit collector geometry used in the simulations.

In the absence of an energy barrier to deposition, the distribution of attached colloids was random across the upstream zones of the collector surfaces, as determined by superposition of the simulated locations of attachment of colloids onto the various unit collectors (Figure 1). In contrast, the distribution of retained colloids in the presence of an energy barrier to deposition was discretely patterned, as described below.

Presence of Energy Barrier. Two dominant mechanisms of colloid retention were demonstrated in the simulations in the presence of an energy barrier to deposition: (1) wedging and (2) retention in zones of flow stagnation. These two mechanisms likely dominate in actual porous media in the presence of an energy barrier, given that (1) the accumulated experimental evidence that points specifically to these mechanisms (12–15, 22, 23); (2) observed colloid deposition efficiencies in porous media are factors of 2–50 or more greater than deposition efficiencies on comparable flat surfaces (12–15) despite the expectation of similar surface

heterogeneity in these two systems; and 3) that the majority of retention is reversed with decreased ionic strength (12–15), which is not consistent with attachment at surface heterogeneities.

The process of wedging is demonstrated by a 0.4 millisecond portion of a simulated colloid trajectory in Figure 2. About 275.8 milliseconds after entering the unit collector, the $18\ \mu\text{m}$ (radius) colloid was in secondary energy minimum association with two collector surfaces, as shown by the slight attraction (FCOLL1 and FCOLL2) and small separation distances (H1 and H2) to two both surfaces (grain to grain contact). The diffusion force (ranging up to 1×10^{-11} N) was insufficient to drive the colloid through the energy barrier, whereas the fluid drag force overwhelmed the repulsive interaction force, leading to strong primary minimum interactions with one collector and attachment to that surface. By superimposing the coordinates of retained colloids, we observe that all colloids retained via wedging were retained at grain to grain contacts (Figure 3). Note that attached colloids located on the outside of the unit collector were wedged between the center spheres of the unit collector shown and the adjacent unit collector.

The process of retention in zones of flow stagnation is demonstrated by a 22 s portion of a simulated colloid trajectory in Figure 4. When the $0.55\ \mu\text{m}$ particle approached the repulsive surface, an equilibrium separation distance (H) was achieved where the attractive van der Waals forces (FVDW) balanced the repulsive electric double layer forces (FEDL). The attractive force was only on the order of 1×10^{-12} N, whereas the diffusion forces ranged up to 1×10^{-9} N (not shown). The apparent magnitude of the diffusion force is misleading, since it is inversely proportional to time step size; whereas, the randomness of diffusion mitigates the impact of the apparently large force over the series of time steps. The randomness of diffusion allowed continued retention of the colloid in the secondary energy minimum, and the particle translated along the collector surface at the equilibrium separation distance corresponding to the sec-

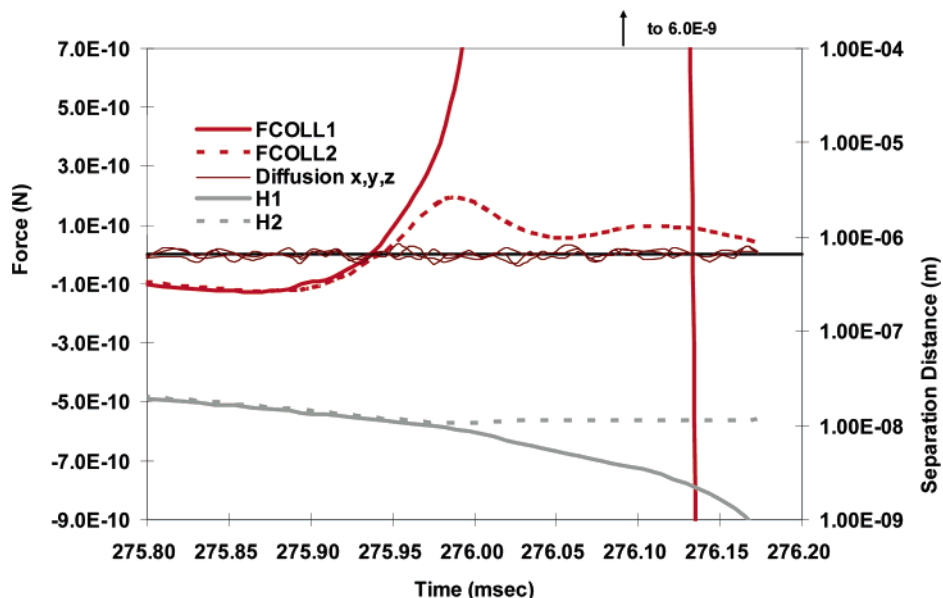


FIGURE 2. Wedging of an $18\ \mu\text{m}$ microsphere in a grain to grain contact as demonstrated via a simulated trajectory (superficial velocity $= 4.0 \times 10^{-4}\ \text{m s}^{-1}$, collector radius $= 390\ \mu\text{m}$, ionic strength $= 0.001\ \text{M}$). FCOLL1 and FCOLL2 are the colloid–surface interaction forces for the first and second collectors encountered, respectively. Diffusion x,y,z refers to the random diffusion force in the x -, y -, and z -dimensions. H1 and H2 are the colloid–surface separation distances for the first and second collectors encountered, respectively.

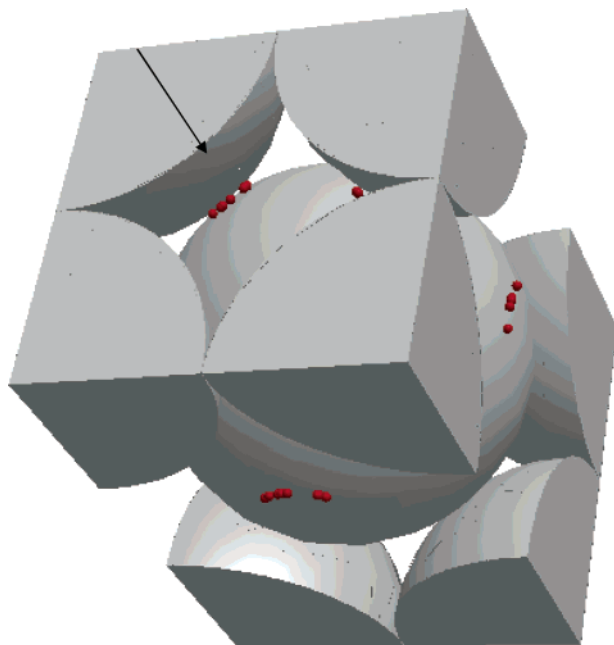


FIGURE 3. Distribution of wedged colloids in the presence of an energy barrier to deposition in the DC unit collector (entry plane $z = -1.414$). The distribution was developed by superimposing onto the unit collectors the locations of wedged colloids determined in the simulations. Note that attached colloids located on the outside of the unit collector were wedged between the center spheres of the unit collector shown and the adjacent unit collector. Arrow denotes direction of flow in z -dimension. Colloid and collectors are not proportionally scaled.

ondary energy minimum. As the particle translated across the surface, it intercepted a zone of flow stagnation, where it was retained, as shown by superimposing coordinates of colloids that were retained without attachment (Figure 5).

Deposition efficiency via wedging is shown in Figure 6 (top) as a function of colloid size and unit collector, where the deposition efficiency (α) is the ratio of the collector efficiency (η) in the presence relative to the absence of an energy barrier to deposition. The trend in α versus colloid

radius demonstrates that wedging operates for relatively large colloids and for relatively high fluid velocities, e.g., with colloid:collector ratios greater than about 0.02 at the $1.71 \times 10^{-5}\ \text{m s}^{-1}$ superficial velocity and colloid:collector ratios greater than about 0.006 at the $4.0 \times 10^{-4}\ \text{m s}^{-1}$ superficial velocity (Figure 6 top), reflecting fluid drag as the driver of wedging. Under the conditions examined, the simulations indicated that wedging did not occur in SC unit collector. However, wedging was simulated in the SC unit collector for larger colloid:collector size ratios (e.g., a ratio of 0.25 at the $1.71 \times 10^{-5}\ \text{m s}^{-1}$ superficial velocity).

Deposition efficiency via retention in flow stagnation zones is shown as a function of colloid size and unit collector (Figure 6, bottom). The trend in α versus colloid radius indicates that retention in flow stagnation zones occurs for colloid:collector ratios less than about 0.002 for both the $4.0 \times 10^{-4}\ \text{m s}^{-1}$ superficial velocity and the $1.71 \times 10^{-5}\ \text{m s}^{-1}$ superficial velocity (Figure 6, bottom), with the magnitude of retention decreasing with increasing fluid velocity. That increased fluid velocity decreased retention via flow stagnation (holding other conditions constant) suggests that the volumes of the flow stagnation zones were reduced with increasing fluid velocity. Retention in flow stagnation zones increased with decreasing colloid size up to a maximum for colloid radii between 0.1 and $0.55\ \mu\text{m}$ radius (Figure 6, bottom). The overall trend reflects the ability of smaller colloids to better “find” flow stagnation zones via diffusion and to exit them via diffusion (smallest colloids). Retention in flow stagnations zones did not occur in the DC unit collector simulations under the 0.001 M ionic strength condition; however, simulated colloid retention in zones of flow stagnation in the DC unit collector did occur at higher ionic strength (discussed below).

The simulated values of α (via wedging and flow stagnation) are sensitive to the height of the energy barrier to deposition (Figure 7, top), thereby confirming the ability of the model to incorporate the influence of colloid–surface interactions. This stands in contrast to the simulations of Cushing and Lawler (24), which did not display sensitivity to an energy barrier. The reason for the differences between our work from that of Cushing and Lawler (24) is not clear. Cushing and Lawler (24) did not include colloid diffusion in

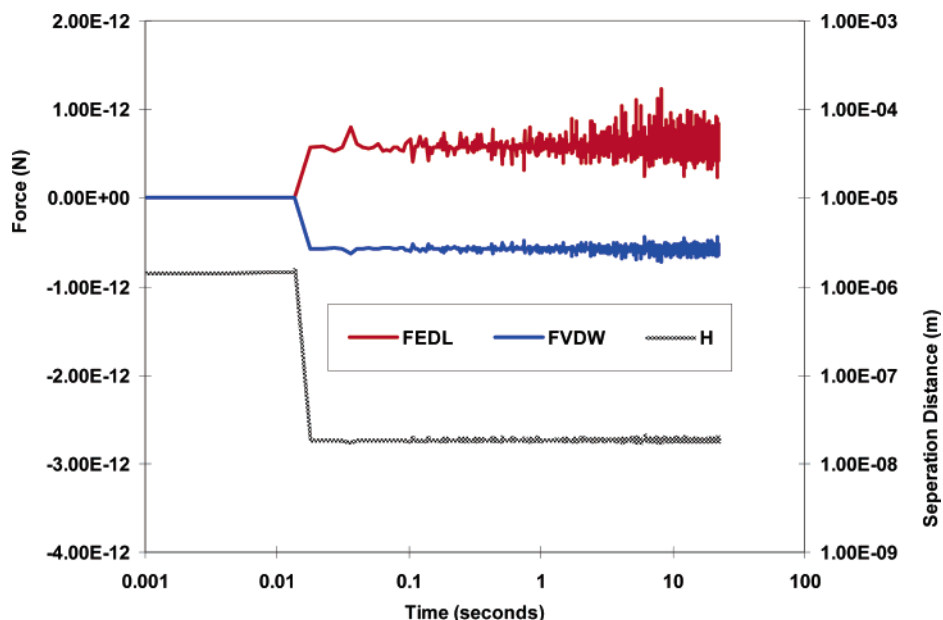


FIGURE 4. Retention of a $0.55\ \mu\text{m}$ microsphere in a flow stagnation zone as demonstrated via a simulated trajectory (superficial velocity $= 4.0 \times 10^{-4}\ \text{m s}^{-1}$, collector radius $= 255\ \mu\text{m}$, ionic strength $= 0.001\ \text{M}$). FEDL is the electric double layer force, FVDW is the van der Waals force, and H is the colloid–collector separation distance.

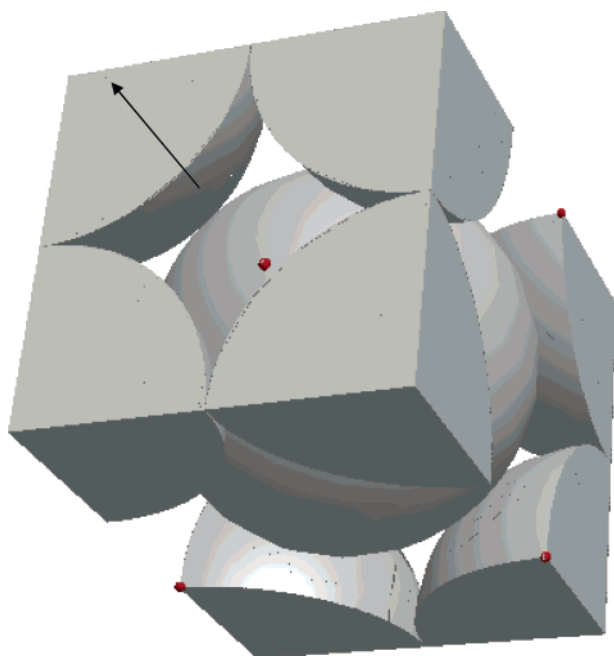


FIGURE 5. Distribution of colloids retained in flow stagnation zones in the presence of an energy barrier to deposition in the DC unit collector (entry plane $z = -1.414$). The distribution was developed by superimposing onto the unit collectors the locations of colloids remaining stationary despite remaining unattached in the simulations. Arrow denotes direction of flow in z -dimension. Colloid and collectors are not proportionally scaled.

their model; however, that difference may not explain the different sensitivities to colloidal interactions between the two models. Cushing and Lawler approximated the DC unit collector fluid velocity field of Sorenson and Stewart (31) to match the velocity expressions used by Rajagopalan and Tien (37); however, it is not clear whether this approximation could lead to the observed insensitivity to colloid–surface interaction.

The sensitivity of simulated colloid retention to colloid–surface interactions is also shown for the secondary energy minimum. The simulated values of α increase with increasing

secondary energy minimum depth (Figure 7, bottom), as shown for the $0.55\ \mu\text{m}$ colloids ($1.71 \times 10^{-5}\ \text{m day}^{-1}$ superficial velocity) in the DC unit collector with entry $z = -1.414$. The result is due to greater association of colloids with surfaces with increased secondary energy minimum depth.

Increased secondary energy minimum depth also increased deposition via wedging, as shown for the $5.0\ \mu\text{m}$ colloids ($4.0 \times 10^{-4}\ \text{m day}^{-1}$ superficial velocity in the DC unit collector with entry $z = -1.414$) (Figure 7, bottom), which is also expected on the basis of greater accumulation of secondary minimum-associated colloids, increasing the probability of such colloids entering grain to grain contacts and wedging between the two collector surfaces.

Discussion

The simulations presented here indicate that Bradford et al. (10) correctly perceived an important change in the mechanism of deposition for colloid:collector size ratios greater than about 0.005. The simulations also elucidate a specific mechanistic basis for the capture of these particles and distinguish the mechanism of capture from the traditional definition of straining. The traditional definition of straining is the trapping of colloid particles in pore throats that are too small to allow particle passage (e.g., 10, 38, 39), whereas the capture mechanism demonstrated here may be more precisely termed wedging, and can be defined as capture via confinement between two bounding surfaces (e.g., 5). This distinction is useful since straining (as traditionally defined) would be expected to plug pore throats and to retain the vast majority of colloids near the entry surface of the porous media (8), whereas wedging would not.

The simulations presented here corroborate recent direct observation of wedging in grain to grain contacts ($18\ \mu\text{m}$ colloids, $390\ \mu\text{m}$ spherical collectors, $4.0 \times 10^{-4}\ \text{ms}^{-1}$ superficial velocity) in the presence of an energy barrier (23). Simulations of these conditions produced corresponding values of α that bracketed the observed value (0.02), i.e., $\alpha < 0.001$ (SC unit collector) and $\alpha = 0.1$ (DC unit collector) (Supporting Information). The inferred retention of secondary-minimum associated colloids in flow stagnation zones in experiments (12–15) is also demonstrated in the mechanistic simulations. That smaller colloids generally yield greater

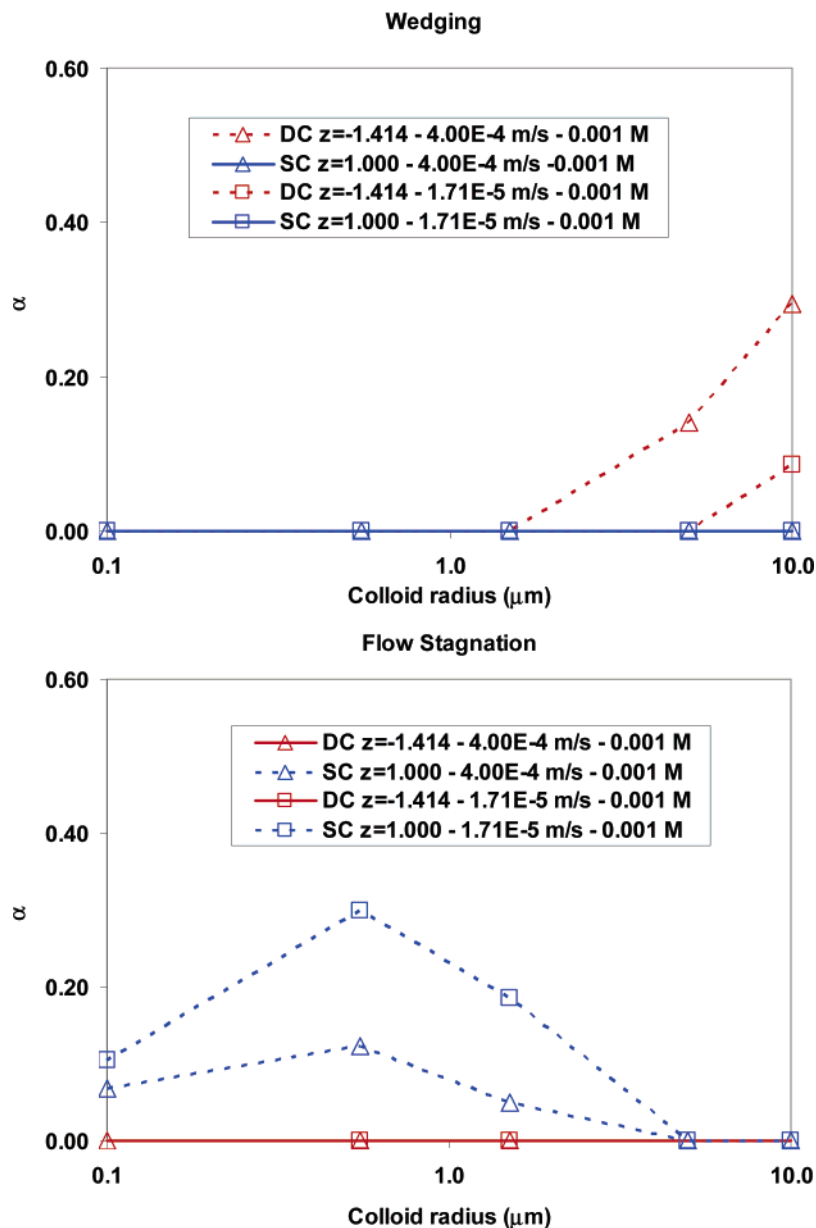


FIGURE 6. Retention (deposition) efficiency (α) (ratio of collector efficiency in presence relative to absence of energy barrier) in the four unit collectors as a function of colloid radius for wedging (top) and retention in flow stagnation zones (bottom). Simulations were conducted for two superficial velocities at an ionic strength of 0.001 M.

retention via flow stagnation is consistent with the recent experimental observation that excess deposition was greatest for the smallest colloids in the range between 0.1 and 2.0 μm (15). However, in the simulations (SC unit collector, entry plane $z = 1$) the smallest colloids (0.1 μm) showed decreased retention relative to the 0.55 μm colloids (Figure 6, bottom), presumably due to greater diffusion translations that were sufficient to remove these colloids from the secondary energy minimum. The simulations do not account for colloid–colloid interactions, which may limit the number of colloids that can be retained in the flow stagnation zones. The limited volume of flow stagnation zones is indicated in simulations by the lack of retention of colloids larger than about 2–5 μm in radius (superficial fluid velocity $1.71 \times 10^{-5} \text{ m s}^{-1}$) (Figure 6, bottom). Despite this expected limit, the number of flow stagnation zones in a given porous media may yield significant overall colloid retention. Furthermore, we use the term “flow stagnation zone” provisionally to represent retention via secondary energy minima, since colloid retention may also potentially occur via secondary minimum

interaction with attached or retained colloids in addition to collectors. Incorporation of colloid–colloid interaction is a challenge involving the communication between parallel processors during simulations.

That colloid deposition efficiencies decrease with increasing fluid velocity in the presence of an energy barrier to deposition (41) is also demonstrated in the simulations for colloids of radii less than about 5 μm (colloid:collector ratios less than 0.02), due to decreasing retention in flow stagnation zones with increasing fluid velocity (shown by comparison of α across fluid velocities for a given unit collector and ionic strength, Supporting Information). Notably, this trend is also expected for the case of deposition via local elimination of the energy barrier due to surface charge heterogeneity or roughness, due to the small size of these hetero-domains relative to the colloid (19).

The distinction between attachment and straining that has been made in recent literature (e.g., 40) can be clarified by the simulations. Wedging and straining are attachment in the presence of an energy barrier, enabled by confinement

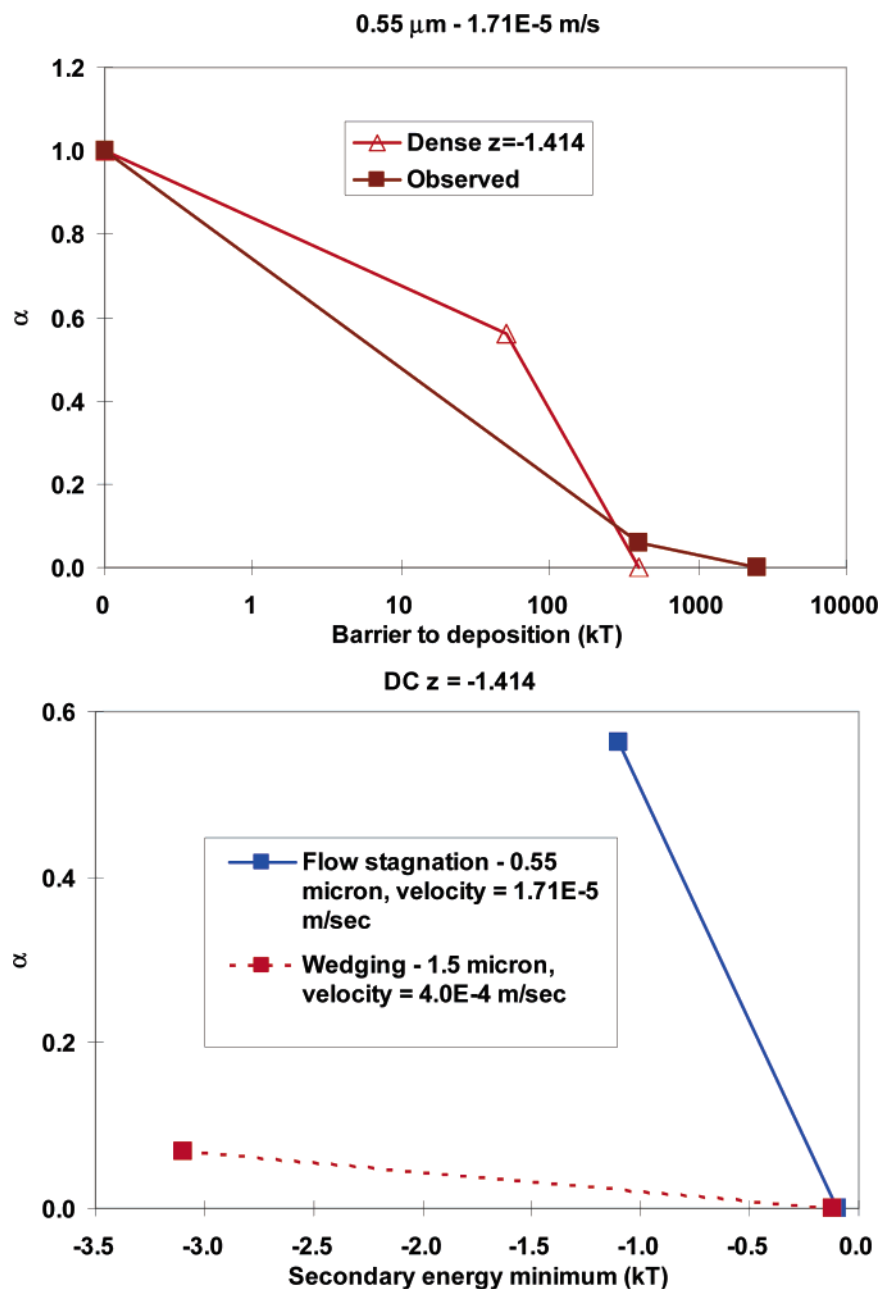


FIGURE 7. Top: Total retention (deposition) efficiency (α) (ratio of collector efficiency in presence relative to absence of energy barrier) via combined wedging and retention in flow stagnation zones in the DC unit collector as a function of height of the energy barrier to deposition, which was manipulated via ionic strength. Observed values are from Li et al. (36). Bottom: Retention (deposition efficiency) (α) via wedging versus retention in flow stagnation zones in the DC unit collector as a function of depth of the secondary energy minimum, which was manipulated via ionic strength.

of the colloid between bounding surfaces: two in the case of wedging, and three or more in the case of straining. Increased secondary energy minimum depth increased colloid translation along the collector surfaces and led to increased wedging and retention in flow stagnation zones (Figure 7, bottom), explaining the observed (in experiments) sensitivity of colloid deposition to colloid–interaction forces despite the presence of a formidable energy barrier. Colloids that are retained do not pass over the energy barrier, but they rather translate along the surfaces in secondary-minimum association with the surface until they become (1) wedged in a grain to grain contact, or (2) retained in a flow stagnation zone, or (3) attached where the energy barrier has been removed or eliminated. Note that experiments indicate that this third mechanism is relatively minor in porous media (12–15). Retention in flow stagnation zones

is not attachment, and as such it is relatively reversible (12–15).

The mechanisms of deposition demonstrated here (i.e., retention in flow stagnation zones and wedging in grain to grain contacts) display different dependencies on fluid velocity, colloid size (Figure 6), and colloid–surface interaction forces (Figure 7), providing a potential explanation of the difficulty in generalizing deposition behaviors among different colloids, as reviewed recently by Tufenkji et al. (39). These mechanisms, along with surface heterogeneity, lay a foundation for mechanistic prediction of colloid retention in the presence of an energy barrier, one that can be potentially up-scaled via a correlation equation for ready prediction of colloid retention in porous media in the presence of an energy barrier. This goal requires determination of representative unit collectors that yield quantitative

values of η and α , or alternatively, requires interfacing particle tracking models to complex fluid velocity fields, e.g., fluid velocity fields developed for pore domains rendered from actual porous media (e.g., via X-ray microtomography). An additional challenge will be the development of dimensionless parameters relating pore domain geometry attributes such as the length and number of grain to grain contacts (22, 23) to readily measured parameters such as grain size distribution and grain shape. The mechanisms of deposition elucidated here also provide a basis for mechanistic understanding of enhanced colloid deposition at sediment textural interfaces, where pore domain geometry at the interface between textural units differs from within the bounding units. An ability to mechanistically simulate colloid retention at textural interfaces will eventually yield improved models of colloid transport in heterogeneous media.

Acknowledgments

This article is based upon work supported by the National Science Foundation Hydrologic Sciences Program (EAR 0337258). Any opinions, findings, and conclusions or recommendations expressed in this material are those of the author(s) and do not necessarily reflect the views of the National Science Foundation. We thank Martin Cuma and Dr. Julio Facelli at the Center for High Performance Computing at the University of Utah for their expert support. We also thank two anonymous reviewers for their helpful comments during review of this manuscript.

Supporting Information Available

Supporting Information is provided regarding the development and implementation of governing equations for the particle trajectory model, fluid velocities, hydrodynamic correction functions, results of simulations in the absence of an energy barrier, and tabular results for all simulations.

Literature Cited

- Elimelech, M.; O'Melia, C. R. Kinetics of deposition of colloidal particles in porous media. *Environ. Sci. Technol.* **1990**, *24* (10), 1528–1536.
- Bhattacharjee, S.; Ko, C. H. Elimelech, M. DLVO interaction between rough surfaces. *Langmuir* **1998**, *14*, 3365–3375.
- Bhattacharjee, S.; Ryan, J. N.; Elimelech, M. Virus transport in physically and geochemically heterogeneous subsurface porous media. *J. Contam. Hydrol.* **2002**, *57*, 161–187.
- Shellenberger, K.; Logan, B. E. Effect of molecular scale roughness of glass beads on colloidal and bacterial deposition. *Environ. Sci. Technol.* **2002**, *36* (2), 184–189.
- Herzig, J. P.; Leclerc, D. M.; LeGoff, P. Flow of suspension through porous media: application to deep filtration. *Ind. Eng. Chem* **1970**, *62*, 129–157.
- Sakthivadivel, R. *Theory and mechanism of filtration of non-colloidal fines through a porous medium*; Hydraulic Engineering Laboratory, University of California, Berkeley, 1966.
- Sakthivadivel, R. *Clogging of a granular porous medium by sediment*; Hydraulic Engineering Laboratory, University of California, Berkeley, 1969.
- Bradford, S. A.; Yates, S. R.; Bettahar, M.; Simunek, J. Physical factors affecting the transport and fate of colloids in saturated porous media. *Water Resour. Res.* **2002**, *38* (12), 1327–1338.
- Bradford, S. A.; Simunek, J.; Bettahar, M.; Genuchten, M. T.; Van Yates, S. R. Modeling colloid attachment, straining, and exclusion in saturated porous media. *Environ. Sci. Technol.* **2003**, *37*, 2242–2250.
- Bradford, S. A.; Bettahar, M.; Simunek, J.; van Genuchten, M. Th. Straining and attachment of colloids in physically heterogeneous porous media. *Vadose Zone J.* **2004**, *3*, 384–394.
- Bradford, S. A.; Simunek, J.; Bettahar, M.; Tadassa, Y. F.; van Genuchten, M. T.; Yates, S. R. Straining of colloids at textural interfaces. *Water Resour. Res.* **2005**, *41*, DOI: 10.1029/2004WR003675.
- Redman, J. A.; Walker, S. L.; Elimelech, M. Bacterial adhesion and transport in porous media: role of the secondary energy minimum. *Environ. Sci. Technol.* **2004**, *38*, 1777–1785.
- Walker, S. L.; Redman, J. A.; Elimelech, M. Role of Cell Surface Lipopolysaccharides (LPS) in Escherichia coli K12 Adhesion and Transport. *Langmuir* **2004**, *20*, 7736–7746.
- Brow, C.; Li, X.; Ricka, J.; Johnson, W. P. Comparison of microsphere deposition in porous media versus simple shear systems. *Colloids Surf. A* **2005**, *253*, 125–136.
- Tong, M.; Johnson, W. P. Excess colloid retention in porous media as a function of colloid size, fluid velocity, and grain angularity. *Environ. Sci. Technol.* **2006**, *40* (24), 7725–7731.
- Franchi, A.; O'Melia, C. R. Effects of natural organic matter and solution chemistry on the deposition and reentrainment of colloids in porous media. *Environ. Sci. Technol.* **2003**, *37*, 1122–1129.
- Hahn, M. W.; O'Melia, C. R. Deposition and reentrainment of brownian particles in porous media under unfavorable chemical conditions: some concepts and applications. *Environ. Sci. Technol.* **2004**, *38* (1), 210–220.
- Hahn, M. W.; Abadzic, D.; O'Melia, C. R. Aquasols: On the role of secondary minima. *Environ. Sci. Technol.* **2004**, *38* (22), 5915–5924.
- Johnson, W. P.; Tong, M. Observed and simulated fluid drag effects on colloid deposition in the presence of an energy barrier in an impinging jet system. *Environ. Sci. Technol.* **2006**, *40* (16), 5015–5021.
- Spielman, L. A.; Cukor, P. M. Deposition of non-Brownian particles under colloidal forces. *J. Colloid Interface Sci.* **1973**, *43* (1), 51–65.
- Tufenkji, N.; Ryan, J. N.; Harvey, R. W.; Elimelech, M. Transport of Cryptosporidium Oocysts in porous media: role of straining and physicochemical filtration. *Environ. Sci. Technol.* **2004**, *38*, 5932–5938.
- Li, X.; Lin, C. L.; Miller, J.; Johnson, W. P. Pore-scale observation of microsphere deposition at grain-grain contacts over assemblage-scale porous media domains using X-ray microtomography. *Environ. Sci. Technol.* **2006**, *40* (12), 3762–3768.
- Li, X.; Lin, C. L.; Miller, J.; Johnson, W. P. Role of grain to grain contacts on profiles of retained colloids in porous media in the presence of an energy barrier to deposition. *Environ. Sci. Technol.* **2006**, *40* (12), 3769–3774.
- Cushing, R. S.; Lawler, D. F. Depth filtration: fundamental investigation through three-dimensional trajectory. *Environ. Sci. Technol.* **1998**, *32*, 3793–3801.
- Payatakes, A. C.; Rajagopalan, R.; Tien, C. On the use of Happel's Model for filtration studies. *J. Coll. Int. Sci.* **1974**, *49* (2), 321–325.
- Payatakes, A. C.; Tien, C.; Turian, R. M. Trajectory calculation of particle deposition in deep bed filtration. *AIChE J* **1974**, *20* (5), 889–899.
- Paraskeva, C. A.; Burganos, V. N.; Payatakes, A. C. Three-dimensional trajectory analysis of particle deposition in constricted tubes. *Chem. Eng. Sci.* **1991**, *108*, 23–48.
- Burganos, V. N.; Paraskeva, C. A.; Payatakes, A. C. Three-dimensional trajectory analysis and network simulation of deep bed filtration. *J. Colloid Interface Sci.* **1992**, *148* (1), 167–181.
- Burganos, V. N.; Paraskeva, C. A.; Christofides, P. D.; Payatakes, A. C. Motion and deposition of non-Brownian particles in upflow collectors. *Sep. Technol.* **1994**, *4*, 47–54.
- Snyder, L. J.; Stewart, W. E. Velocity and pressure profiles for newtonian creeping flow in regular packed beds of shapes. *AIChE J* **1966**, *12* (1), 161–173.
- Sorensen, J. P.; Stewart, W. E. Computation of forced convection in slow flow through ducts and packed beds-1 extensions of the graetz problem. *Chem. Eng. Sci.* **1974**, *29*, 811–817.
- Brenner, H. The slow motion of a sphere through a viscous fluid towards a plane surface. *Chem. Eng. Sci.* **1961**, *16*, 242–251.
- O'Neill, M. N. A sphere in contact with a plane wall in a slow linear shear flow. *Chem. Eng. Sci.* **1968**, *23*, 1293–1298.
- Goldman, A. J.; Cox, R. G.; Brenner, H. Slow viscous motion of a sphere parallel to a plane wall-II couette flow. *Chem. Eng. Sci.* **1967**, *22*, 653–660.
- Goldman, A. J.; Cox, R. G.; Brenner, H. Slow viscous motion of a sphere parallel to a plane wall-I motion through a quiescent fluid. *Chem. Eng. Sci.* **1967**, *22*, 637–651.
- Li, X.; Scheibe, T. D.; Johnson, W. P. Apparent decreases in colloid deposition rate coefficient with distance of transport under unfavorable deposition conditions: a general phenomenon. *Environ. Sci. Technol.* **2004**, *38* (21), 5616–5625.
- Rajagopalan, R.; Tien, C. Trajectory analysis of deep-bed filtration with the sphere-in-cell porous media model. *AIChE J* **1976**, *22* (3), 523–533.

- (38) McDowell-Boyer, L. M.; Hunt, J. R.; Sitar, N. Particle transport through porous media. *Wat. Resour. Res.* **1986**, *22*, 1901–1921.
- (39) Tufenkji, N.; Dixon, D. R.; Considine, R.; Drummond, C. J. Multi-scale cryptosporidium/sand interactions in water treatment. *Wat. Resour. Res.* **2006**, *40*, 3315–3331.
- (40) Bradford, S. A.; Simunek, J.; Bettahar, M.; van Genuchten, M. T.; Yates, S. R. Significance of straining in colloid deposition: evidence and implications. *Wat. Resour. Res.* **2006**, *42*, DOI: 10.1029/2005WR004791.
- (41) Johnson, W. P.; Li, X.; Assemi, S. Hydrodynamic drag Influences deposition and re-entrainment dynamics of microbes and non-

biological colloids during non-perturbed transport in porous media in the presence of an energy barrier to deposition. *Adv. Water Resour.* (Special Issue) **2006**, DOI: 10.1016/j.advwatres.2006.05.020.

Received for review May 30, 2006. Revised manuscript received November 27, 2006. Accepted November 28, 2006.

ES061301X